ACS APPLIED MATERIALS & INTERFACES

Research Article

www.acsami.org

Functionalization of Defect Sites in Graphene with RuO_2 for High Capacitive Performance

Fan Yang,*[,†] Lianbing Zhang,[†] Ana Zuzuarregui,[†] Keith Gregorczyk,[†] Le Li,[†] Mikel Beltrán,[†] Christopher Tollan,[†] Jens Brede,[‡] Celia Rogero,[§,‡] Andrey Chuvilin,[†,∥] and Mato Knez*[,†,∥]

[†]CIC nanoGUNE Consolider, Tolosa Hiribidea 76, 20018 Donostia−San Sebastian, Spain

[§]Donostia International Physics Center, Paseo Manuel de Lardizabal 4, 20018 Donostia−San Sebastian, Spain

[‡]Centro de Física de Materiales, Paseo Manuel de Lardizabal 5, 20018 Donostia−San Sebastian, Spain

[∥]Ikerbasque, Basque Foundation for Science, Maria Diaz de Haro 3, 48013 Bilbao, Spain

Supporting Information

ABSTRACT: Graphene is an attractive material for its physicochemical properties, but for many applications only chemically synthesized forms such as graphene oxide (GO) and reduced graphene oxide (rGO) can be produced in sufficient amounts. If considered as electrode material, the intrinsic defects of GO or rGO may have negative influence on the conductivity and electrochemical properties. Such defects are commonly oxidized sites that offer the possibility to be functionalized with other materials in order to improve performance. In this work, we demonstrate how such ultimately efficient functionalization can be achieved: namely, through controlled binding of very small amount of materials such as RuO_2 to rGO by atomic layer deposition (ALD), in this way substituting the native defect sites with RuO_2 defects. For the example of a supercapacitor, we show that defect functionalization results in significantly enhanced specific capacitance of the electrode and that its energy density can be stabilized even at high consumption rates.

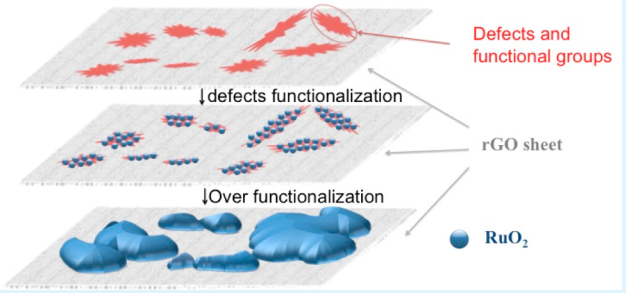

KEYWORDS: *reduced graphene oxide, ruthenium oxide, functionalization, atomic layer deposition, supercapacitors*

1. INTRODUCTION

Graphene is a material with exciting physical properties, and therefore it is of great interest for numerous applications, including but not limited to electronics, energy storage and conversion, etc.[1−6] Although vapor-based synthetic processes for defect-free graphene have been established,[7] wet chemical procedures that yield graphene oxide (GO) in large amounts are most common.[8] The drawback of those materials is their large number of defects, commonly oxidized carbon, that have serious negative impact on the physical or electrochemical properties of this graphitic compound. Chemical reduction of such defects is a common procedure and yields reduced graphene oxide (rGO) that, in spite of still having defect sites, closely resembles the properties of graphene. Functionalization of the remaining defect sites with precise control may be of great benefit for any anticipated application and may pave the way for novel graphene-based devices with high efficiency.

Among applications for which graphene is considered beneficial, supercapacitors attract considerable attention. Supercapacitors are of current interest for their high power density, fast charge/discharge rate, and excellent cycling stability as well as operational safety.[9−12] A serious amount of research and development is devoted to investigation of various types of graphene-based electrodes, including graphene only,[13−15] graphene−metal oxide composites,[16−19] and so on. In a recent work, hydrous RuO_2 particles have been anchored to graphene sheets through sol−gel techniques and low-temperature annealing, eventually resulting in a high specific capacitance of the composite.[18] Such heterogeneous compositions are very interesting from the scientific perspective. Namely, occasionally specific capacitances are observed that are beyond those expected from a theoretical sum of the constituent components. Such additive effects are believed to result from synergies between the materials and may have multiple chemical or physical origins. If one considers rGO, one major reason for deviation of the physicochemical properties from the expected ones may lie in the intrinsic defect sites that affect both conductivity and capacitance of the rGO. Such defects are, however, not easy to chemically modify in a controlled way.

A very precise technology for achieving controlled deposition of numerous materials is atomic layer deposition (ALD). Although it was primarily developed to deposit thin films with extreme precision in thickness, ALD also offers the possibility to grow nanoparticles on a variety of substrates.[20,21] The method relies on chemical half-reactions occurring on a surface upon sequential precursor supply from the vapor phase, and

Received: January 9, 2015
Accepted: September 2, 2015
Published: September 2, 2015

DOI: 10.1021/acsami.5b04704
ACS Appl. Mater. Interfaces 2015, 7, 20513−20519

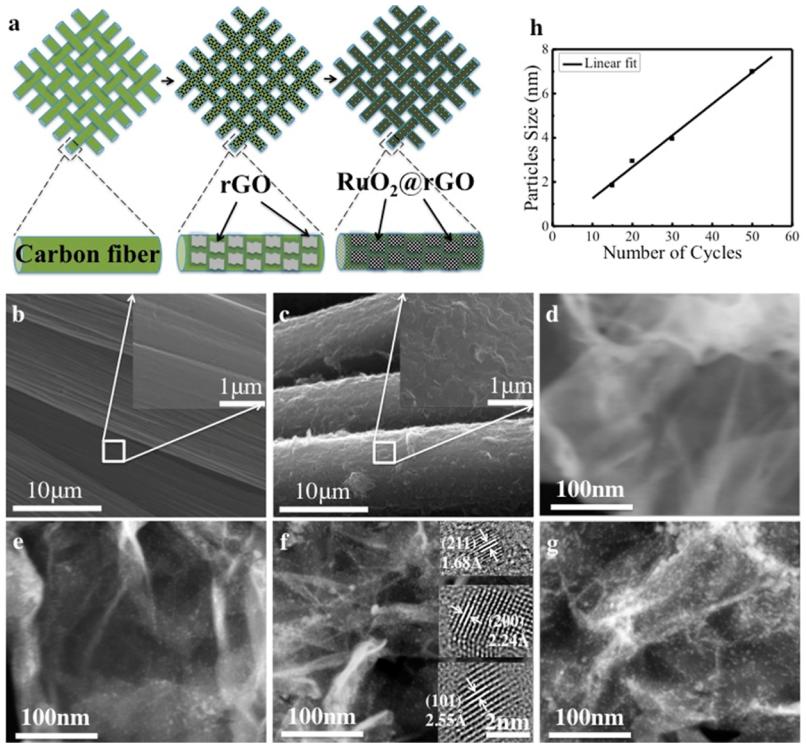

Figure 1. (a) Schematic of fabrication process of rGO/RuO_2 electrodes on carbon cloth. The first step involves attachment of rGO to carbon cloth by electrochemical immobilization (ECI). In the second step, atomic layer deposition (ALD) is applied to deposit RuO_2 nanoparticles on rGO. (b, c) Scanning electron microscope (SEM) images of (b) carbon fiber and (c) carbon fiber covered with rGO (insets, higher magnification). (d–g) Scanning transmission electron microscope (STEM) images of (d) rGO, (e) rGO/RuO_2-15, (f) rGO/RuO_2-20, and (g) rGO/RuO_2-30. The inset in panel f shows HRTEM images of RuO_2 nanoparticles; scale bar 2 nm. (h) Average size dependence of RuO_2 nanoparticle on number of ALD cycles.

therefore it is easily and efficiently applicable even to substrates with complex morphologies; that is, it enables non-line-of-sight deposition. The self-saturating mechanism in ALD processes allows extreme control of the amount of deposited material, even at the atomic scale, by simply controlling the number of deposition cycles. Furthermore, ALD is a chemical process involving covalent bonding of the precursors to the substrate in each half-reaction, allowing for intimate and stable contact of the substrate and deposit. Thus, it would be quite convenient to functionalize the defects of rGO with high accuracy by applying ALD.

The present work shows an approach toward optimization of the electrode material based on the already mentioned system of RuO_2 nanomaterials in combination with rGO. The deposition of tiny amounts of RuO_2 on reduced graphene oxide (rGO) is performed by ALD, with its loading being controlled with the number of processing cycles. We show with the example of a supercapacitor that the resulting composite ultimately exploits synergistic effects, with specific capacitances being close to the theoretically achievable value of 1132 F/g (at 50 mV/s scanning rate). An optimized loading of only ∼9.3 wt % Ru results in ∼40% increase in specific capacitance of the rGO electrodes resulting from testing in a classical two-electrode configuration. Furthermore, the cycling stability of the electrodes is strongly improved. The tight chemical bonding between the RuO_2 particles and the rGO sheet makes the electrodes exhibit excellent cycling performance, with ∼92% retention over 4000 cycles. The improvement is not a priori dependent on the Ru loading, as a further increased amount of Ru results in a drop of the specific capacitance. Therefore, it is more likely that the defect sites of the rGO become functionalized until they are consumed.

2. RESULTS AND DISCUSSION

The anticipated functionalization of rGO is most easily shown by a practical example. Therefore, we chose the supercapacitor as demonstrator and initially fabricated the electrodes. The fabrication process consists of two steps: (1) electrochemical immobilization (ECI) of rGO sheets onto carbon cloth and (2) growth of RuO_2 nanoparticles on the immobilized rGO by ALD (Figure 1a). In more detail, a contacted carbon strip was immersed into an rGO suspension with a gold plate as counter electrode. By applying a constant current to the electrodes, the negatively charged rGO sheets were adsorbed to the surface of the carbon cloth. Figure 1b,c shows the surface morphology changes of carbon electrodes after the ECI process. In Figure 1c, individual carbon fibers fully covered with rGO sheets containing one or more graphene layers can be seen. This process allows intimate binding of rGO to the carbon fiber, thus contributing significantly to both the conductivity and long-term electrochemical stability of the electrode. In addition, the graphene seriously enhances the total electrochemical capacitance of the electrodes, which will be described in detail later. In the forthcoming discussion the capacitance was considered to dominantly originate from the rGO (or rGO/RuO_2), while the capacitance from the carbon cloth substrate was neglected for convenience (see Supporting Information).

In the second step, the rGO was functionalized with RuO_2 by applying an ALD process with $Ru(EtCp)_2$ [bis-(ethylcyclopentadienyl)ruthenium] and O_2 as precursors.[22−26] Commonly, one would expect the deposition of a thin RuO_2

DOI: 10.1021/acsami.5b04704
ACS Appl. Mater. Interfaces 2015, 7, 20513−20519

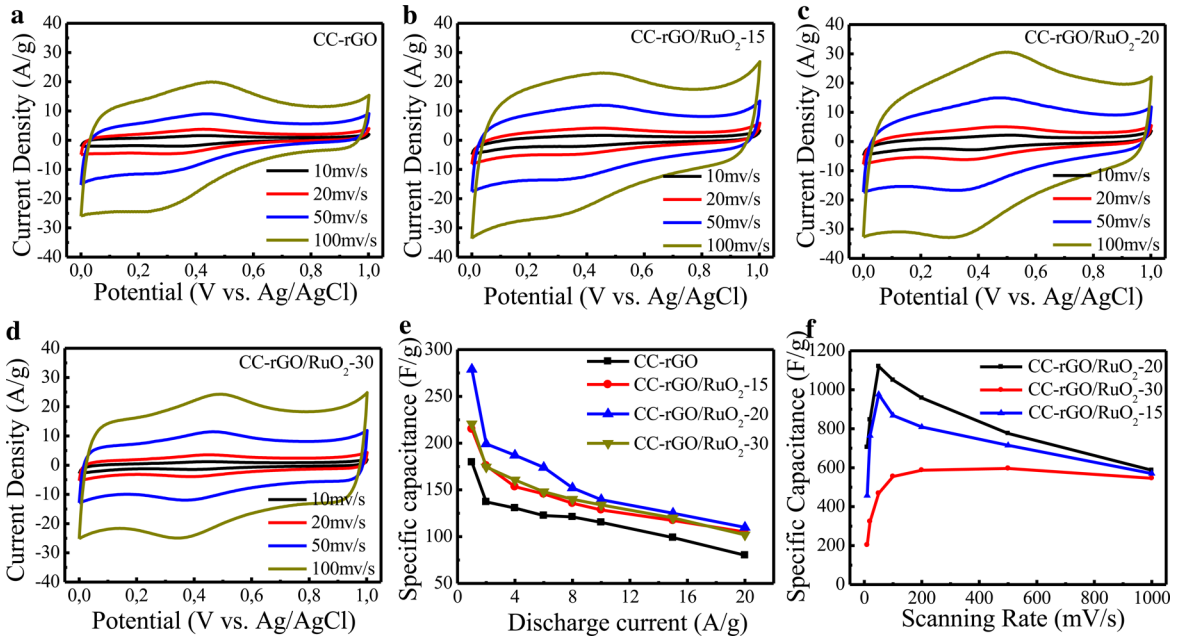

Figure 2. (a–d) Cyclic voltammetry curves of (a) rGO, (b) rGO/RuO_2-15, (c) rGO/RuO_2-20, and (d) rGO/RuO_2-30 at scanning rates of 10, 20, 50, and 100 mV/s each, measured in a three-electrode setup. (e, f) Calculated specific capacitance of (e) composite rGO/RuO_2 and (f) RuO_2 nanoparticles only.

film by ALD,[27] but given the chemical inertness of graphene, the growth of RuO_2 proceeded on distinct sites only. This can be attributed to the chemistry between precursor and substrate: namely, the ALD precursors require a functional site for chemisorption during the first half-reaction. The functional sites are commonly defects, and in the case of oxidized graphene those may be carboxylic or alcoholic functionalities present intrinsically or induced by oxidative pretreatment with plasma or ozone.[28] The distribution of the defects is reflected in the distribution of the RuO_2 nanoparticles on rGO after the ALD process and is very uniform. With fully functional surfaces, a two-dimensional ALD film would grow into the third dimension, that is, the film thickness will be a function of the number of ALD cycles applied. Since the initially deposited RuO_2 on defect sites of the rGO act as zero-dimensional seeds, the growth proceeds in three dimensions, eventually resulting in highly controllable nanoparticle growth. The nanoparticle diameters become a function of the number of applied cycles. Figure 1d–g shows STEM micrographs of rGO and rGO-X (where X = 0, 15, 20, or 30 applied ALD cycles) samples with randomly distributed RuO_2 nanoparticles that grew on rGO. Occasionally, bigger particles were observed. Those are either the result of merging of neighboring particles during growth[27,29] or optical illusions resulting from imaging through semitransparent graphene sheets in folded or overlapped regions of graphene. These seemingly bigger particles become particularly obvious when the ALD cycle numbers increase beyond 30. An example of rGO/RuO_2 after 50 ALD cycles is shown in Figure S1. Once the number of applied ALD cycles increases beyond 50, the nanoparticles merged into a continuous film.

Figure 1h shows an almost perfect linear dependence of the average size of RuO_2 nanoparticles on the number of ALD cycles. One can tune the particle size (and resulting loading) easily by altering the number of ALD cycles applied. Furthermore, the sizes of the grown particles had a very small deviation for each sample (Figure S2). This precise control over the deposited RuO_2 is sine qua non for an optimal functionalization of the defect sites of rGO. The grown RuO_2 particles were characterized by high-resolution transmission electron microscopy (HRTEM), X-ray diffraction (XRD), and Raman spectroscopy. Well-defined crystalline lattice can be clearly seen in the inset of Figure 1f, and lattice spacings of 2.55, 2.24, and 1.68 Å perfectly match the (101), (200), and (211) crystallographic planes of the tetragonal RuO_2 (JCPDS 00-040-1290). XRD and Raman spectroscopic characterization are detailed in the Supporting Information (Figure S3). Note that for Raman spectroscopy and XRD the sample after 50 ALD cycles was used, since the loading of RuO_2 on samples with lower numbers of ALD cycles was too low and resulted in spectra with poor resolution and signal-to-noise ratio. A more precise characterization of the deposited material after fewer cycles is reserved for future studies, as more sophisticated techniques need to be applied and the instrumentation for such characterizations still requires engineering until it becomes operational.

XPS studies were conducted in order to understand the nature of the chemical interaction between RuO_2 particles and rGO substrate. Figure S4a,b shows the O 1s core level spectra where the signal intensity in the low binding energy region significantly increases, which can be attributed to the RuO_2 that formed after ALD functionalization. However, the signal intensity in the higher binding energy region also changed, showing a decrease in region II and, in parallel, an increase in region III. The signals in region II and III predominantly originate from the O in C═O and C−OH, respectively. Note that Ru and H have the same Pauling electronegativity (both 2.2), and therefore C−O−Ru is expected to overlap with C−O−H in region III. A very likely explanation for the increase in signal intensity may be that during the ALD process some of the C═O-type defects in rGO are attacked by the Ru precursor to form C−O−Ru (see details in the Supporting Information). Thus, the ALD functionalization proceeds in a covalent way.

DOI: 10.1021/acsami.5b04704
ACS Appl. Mater. Interfaces 2015, 7, 20513−20519

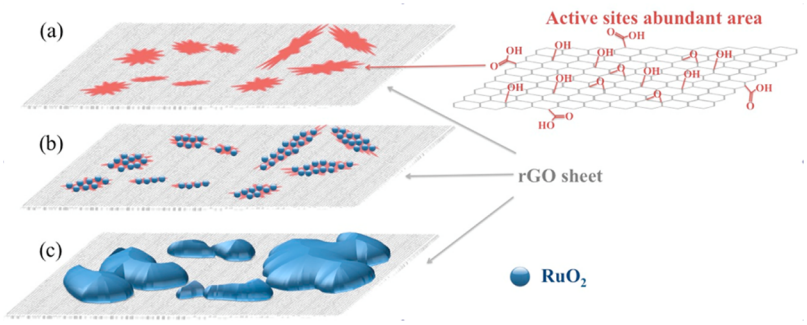

Figure 3. Morphological evolution of ALD-deposited RuO_2 on rGO. (a) rGO sheet with active sites; (b) RuO_2 nanoparticle fully replaces the defects on rGO sheets (corresponding to 20 deposition cycles); (c) RuO_2 nanoparticles merge with closing particles into a bulk RuO_2 (corresponding to 30 or more deposition cycles).

Graphene sheets with different oxidation degree were tested with the same ALD process in order to demonstrate the potential to control the RuO_2 loading with control of defect density. As shown in Figure S5a–d, the density of RuO_2 nanoparticles increased with the oxidation degree (density of defects and functional groups in graphene). This further shows that the ALD functionalization strategy can be applied to graphene oxide in various defect density states and that the ALD growth mechanism drives the particles to grow on defect sites and functional groups. The results are in strong agreement with earlier work, which demonstrated the growth of Pt particles on grain boundaries of graphene grown by chemical vapor deposition (CVD) during the ALD deposition.[30]

The electrochemical capacitive performance of the rGO and rGO/RuO_2-X electrodes was evaluated by cyclic voltammetry (CV) and galvanostatic charge/discharge tests. Figure 2a–d shows CV curves of electrodes containing bare rGO and rGO/RuO_2 after 15, 20, or 30 ALD cycles at potential intervals ranging from 0 to 1 V versus Ag/AgCl. The curves were measured in a three-electrode setup in 1 M aqueous H_2SO_4, and the scanning rates were varied between 10 and 100 mV/s as indicated. In Figure 2a, redox peaks can be observed in the CV of the rGO sample, which can be attributed to defects and chemical functional groups existent on the rGO, which are presumably active sites for redox reactions during the CV scanning. Those defects are most likely the intrinsically present oxidized sites of the rGO. Similar peaks have also been observed in studies of the capacitive performance of carbon nanotube/graphene composites.[31]

As the number of ALD cycles increased, the CV curves of rGO/RuO_2-X electrodes also gradually changed their shape, becoming more symmetric and rectangular (Figure 2a–d). The oxidation peak gradually shifted from around 0.42 V (rGO and rGO/RuO_2-15) to 0.49 V (rGO/RuO_2-20) and further to 0.5 V (rGO/RuO_2-30), which is obviously related to the increasing quantity of RuO_2. The growing RuO_2 nanoparticles substitute the defects and functional groups of the graphene, and thus the oxidation peak can be attributed to the Faradaic electrochemical reaction related to RuO_2.[18,32−34] With higher loading, the contribution of RuO_2 increases. This is particularly expressed with the rGO/RuO_2-30 electrode as depicted in Figure 2d. Here, the CV curve approaches higher symmetry. However, a better performance does not necessarily stand in direct relation to the increasing quantity of RuO_2. The current density showed highest values with samples after 20 RuO_2 deposition cycles. Both higher and lower numbers of cycles resulted in lower current densities. The calculated specific capacitance of rGO and rGO/RuO_2-X, based on charge/discharge measurement in the same three-electrode system, is shown in Figure 2e. The unmodified rGO electrode shows a specific capacitance of 184 F/g at a discharging rate of 1 A/g, which is in agreement with reports from literature.[13] In comparison, the rGO/RuO_2 samples showed a significant increase with the best value being 278 F/g, which is an increase of ∼51%. The corresponding sample was produced with 20 ALD cycles and contained very low amount of RuO_2 (∼9.3 wt % Ru) as measured with inductively coupled plasma mass spectrometry (ICP-MS).

The specific capacitance of the rGO/RuO_2 electrodes does not correlate with the increase in RuO_2 quantity. This may have various reasons. On one hand, the particle size may play an important role. Namely, with increasing particle size, the surface-to-volume ratio of the RuO_2 decreases. Without any doubt, an optimal surface-to-volume ratio of RuO_2 exists. As the Faradaic reaction takes place only at the near surface area, only the RuO_2 located at the surface or in subsurface areas of the particles is involved in the reaction. From the electrochemical point of view, the best performance can be obtained only at a critical point, where the total content of RuO_2 in the nanoparticles is considered as accessible surface species and none or just a minimum of bulk-type RuO_2 is present. Any further increase in RuO_2 quantity will alter this delicate balance with negative impact on the specific capacitance. On the other hand, the interface chemistry of RuO_2 and rGO may have an impact on the capacitance. The oxidized parts of the rGO can be considered defects that affect the capacitance of graphene. Binding Ru to those defects will chemically modify the substrate by substituting C−O sites with C−O−Ru in the first place and subsequently grow further as RuO_2. The nature of the bonding is of critical importance for best possible synergy of the materials. In our case, the bonding is covalent and direct, that is, without linkers or mediators, thus enabling direct electron transfer between the materials. Such synergies between the constituting materials add value to the specific capacitance of the electrode, beyond the theoretical individual contributions of the involved materials.

The specific capacitances of RuO_2 within the samples processed with 15, 20, and 30 ALD cycles were calculated and compared (Figure 2f). The maximum specific capacitance of RuO_2 is observed at a scanning rate of 50 mV/s instead of 10 mV/s, indicating a serious contribution of the active sites to the capacitance at low scanning rates. The RuO_2 nanoparticles grew on defects or functional groups of the rGO, and thus part of the capacitance can be attributed to RuO_2 substituting the

DOI: 10.1021/acsami.5b04704
ACS Appl. Mater. Interfaces 2015, 7, 20513−20519

capacitance of the initial, unaltered active sites. A similar effect has been observed for the specific capacitance of MnO_2 from porous gold/MnO_2 hybrid electrodes.[35] The highest value for the specific capacitance of RuO_2 was 1132 F/g, which is very close to the theoretical value (1300−1500 F/g).[32,36] A very interesting relationship between specific capacitance and number of ALD cycles can be observed in Figure 2f; namely, the peak values are highest with samples processed with 20 cycles, while higher and lower cycle numbers result in lower peak values. This peculiar behavior indicates that the composite undergoes a modification more complicated than the simple attachment of nanoparticles to the substrate and their growth. Although further investigations have to be performed in order to gain more clarity, we propose that the initial deposition of RuO_2 with only a few ALD cycles results in an increasing replacement of oxidized carbon groups on defect sites with Ru, thus altering the effects of the intrinsic defects of the rGO. The deposited RuO_2 is fully accessible for the Faradaic reaction and enhances the specific capacitance of the electrode. With 20 cycles, a peak value is reached, which indicates that nearly all defect sites have been saturated with RuO_2 (Figure 3b). Further deposition of RuO_2 emphasizes the RuO_2 contained in the growing nanoparticles rather than the fraction bound to rGO on the expense of the specific capacitance (Figure 3c).

We chose the above-mentioned rGO/RuO_2-20 electrode to further study the properties under more realistic conditions, that is, in a classical two-electrode configuration with filter paper as separator and 1 M aqueous H_2SO_4 as electrolyte. In contrast to the CV curves of the bare rGO electrodes (Figure 4a), the rGO/RuO_2-20 samples show an almost perfect symmetric rectangular shape, characteristic of a perfect capacitor (Figure 4b). Obviously, the rGO/RuO_2 composite absorbs the H^+ cations in a fast, reversible, and successive way, showing its great suitability as electrode for electrochemical capacitors. The absence of redox peaks can be explained with the devices having been charged and discharged at a pseudoconstant rate over the entire voltammetric range.[35] Resulting from the galvanostatic charge/discharge test (Figure S8), the specific capacitances of rGO and rGO/RuO_2-20 were calculated to be 106 and 148 F/g, respectively, at a 1 A/g discharging rate (Figure S8). Although the increase of ∼40% is somewhat lower than the ∼51% obtained with the three-electrode setup, it is significant, particularly in view of the very low amount of material loaded.

For a better comparison and evaluation of RuO_2 utilization, the individual contributions of RuO_2 and rGO to the energy density of the electrode at the designated values of power density are shown in the Ragone plot in Figure 4d. Given the significantly lower loading with RuO_2, the total energy density of our composite is lower than that of the composites described in relevant literature (Figure S9). The more interesting aspect is, however, related to the individual contributions of the constituent materials of the composite. A closer look at the bars in Figure 4d reveals that the total energy density is composed of significant contributions of rGO and RuO_2, indicating serious exploitation of both constituents. A more peculiar effect can be seen from the lower, black parts of the columns, showing the specific energy density contribution by RuO_2. While commonly with higher power consumption rates the energy density decays (see Figure S9 for further rGO/RuO_2 composites), our composite shows a compensation of the loss related to the rGO by RuO_2, thus stabilizing the electrode toward higher power densities. Namely, with increasing power density, the

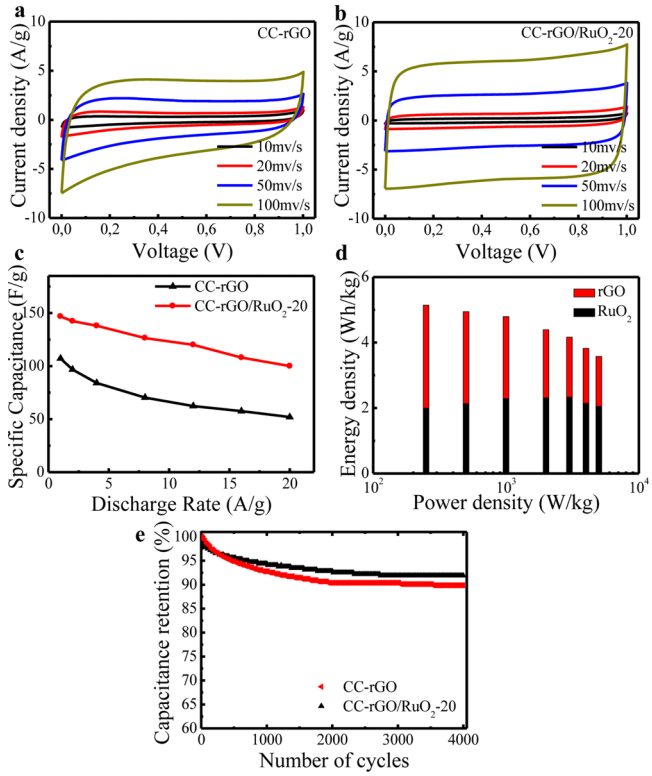

Figure 4. (a, b) Cyclic voltammetry curves of (a) rGO and (b) rGO/RuO_2-20 at different scanning rates, measured in a two-electrode configuration. (c) Calculated specific capacitance of rGO and rGO/RuO_2-20. (d) Ragone plot of energy density vs power density of this work, indicating the individual contributions of rGO and RuO_2 to the energy density. (e) Cycling stability of rGO and rGO/RuO_2-20 electrodes, measured by cyclic voltammetry at a scanning rate of 100 mV/s.

contribution of RuO_2 to the specific energy density increases to a peak value and subsequently decreases again. We ascribe this effect to the defect-optimized rGO. Namely, the oxidized carbon sites are nearly fully replaced with RuO_2, which is fully involved in the Faradaic reaction. This effect has not been observed before. At a high power consumption rate, bigger or nonuniform particles, such as those reported in the literature (Figure S9), contain RuO_2 that apparently is not fully involved in the Faradaic reaction but to a great extent acts as an electronic conductor only.

In addition to the size control, another great advantage of the ALD approach lies in the chemical bonding of RuO_2 nanoparticles to graphene sheets, which is intrinsic to ALD processes. This tight chemical bonding can largely prevent the agglomeration of RuO_2 nanoparticles, which is one of the major obstacles causing performance degradation of supercapacitors based on nanoparticle-related materials or structures. Indeed, the resulting rGO/RuO_2-based device becomes very stable during cycling. Figure 4e shows that the rGO electrodes have a retention of ∼90%, while the rGO/RuO_2-20 electrodes have a value of ∼92% after 4000 CV cycles at a scanning rate of 100 mV/s. These results are significantly higher than those reported in the literature.[17,18,32,36]

3. CONCLUSIONS

In summary, we have demonstrated that ALD is a method of choice for defect management in rGO. The intrinsically present

DOI: 10.1021/acsami.5b04704
ACS Appl. Mater. Interfaces 2015, 7, 20513−20519

oxidized carbon can be precisely modified with functional materials, and in this way the electronic properties can be efficiently altered. For the example of a supercapacitor, a controlled deposition of RuO_2 resulted in electrodes with excellent capacitive performance and stability. This excellent performance is a consequence of the selective chemical binding of RuO_2 to defect sites of the rGO substrate, which changes the chemical nature of those defects. Within the range of a few ALD deposition cycles only, the specific capacitance of the electrode can be maximized, which in realistic circumstances yields an ideal capacitor with stable energy densities over a broad range of power densities. The deposited RuO_2 is tightly bound; thus agglomeration of the formed nanoparticles is prevented. The possibility to identify the optimal loading with RuO_2 and the precise control of growth by ALD allow a more economical fabrication of such composite electrodes in addition to saving resources. Current state-of-the-art ALD instrumentation uses high-speed valves and thus offers good control over the precursor dosing, which in an optimized process allows for decreasing the precursor consumption to a minimum of waste. Combined with simplicity and potential for scaling up toward mass production, ALD has great potential to become the method of choice to modify a range of substrates with various interesting functional materials in a similar way.

4. EXPERIMENTAL SECTION

rGO/RuO_2 Electrode Fabrication. rGO/RuO_2 was fabricated in two steps. First, rGO sheets were electrochemically immobilized onto carbon cloth. For this purpose, carbon cloth with a thickness of about 300 μm (12 mg/cm^2) was cut into rectangular strips (1 cm × 2 cm) to be used as the substrate. Commercially available reduced graphene oxide (rGO) powder (Graphenea, Spain) was dispersed in water (~0.1 mg/mL) with the assistance of ultrasound. One slice of carbon cloth was used as the positive electrode; a gold plate was used as counter electrode. The two electrodes were vertically immersed into the rGO solution in a beaker with a 1 cm distance between the two electrodes. A constant current of 0.25 mA was applied for 5 h. Subsequently, the carbon cloth was removed and dried in air. The weight of the electrode was measured by a microbalance before and after the immobilization. In the second stage, ruthenium oxide was deposited onto rGO sheets by ALD (Savannah 100, Cambridge).[22−26] The reactor was kept at 250 °C, while the ruthenium precursor $Ru(EtCp)_2$ was maintained at 75 °C. High-purity O_2 (99.99%) was used as oxygen source, and high-purity N_2 (99.99%) was used as carrier gas and purging gas. All gas lines were kept at 130 °C to prevent cold spots and precursor condensation. For each ALD cycle, the pulse time, exposure time, and purging time of $Ru(EtCp)_2$ and O_2 precursors were 1 s/60 s/90 s and 3 s/60 s/90 s, respectively. The size of the RuO_2 particles was accurately controlled by the number of ALD cycles, and the loadings were quantified by inductively coupled plasma mass spectrometry (ICP-MS, NexION 300).

Physical Characterization. The morphologies and microstructures of all prepared samples were examined by scanning electron microscopy (FEI, Quanta 250 FEG) and transmission electron microscopy (FEI, Titan G2 60−300) at various magnifications. XRD examinations were performed with a powder diffractometer (X'pert, PANalytical). Raman spectroscopy was performed by use of a Raman microscope (Alpha 300S, WITec). XPS experiments were performed on a Phoibos photoelectron spectrometer equipped with an Al Kα X-ray source (12 mA, 8.33 kV) for the incident photon radiation. Tantalum foil was used to create an electrical contact between the sample surface and the sample holder to avoid charging effects and also acted as calibration of the binding energy.

Electrochemical Characterization. All prepared electrodes were first tested in a three-electrode cell, where a Pt sheet served as the counter electrode, Ag/AgCl (3 M KCl) as the reference electrode, and 1 M H_2SO_4 aqueous solutions as the electrolyte. Cyclic voltammetry curves were recorded in a potential range between 0 and 1 V at various scanning rates. The galvanostatic charge/discharge processes were performed from 0 to 1 V at different current densities. Both CV tests and galvanostatic charge/discharge tests were also performed in a classical two-electrode configuration, where two rGO/RuO_2-20 electrodes (or rGO electrodes) were assembled into a supercapacitor device with laboratory filter paper (Carl Roth, Germany) as separator in 1 M H_2SO_4 aqueous solution. The cycling stabilities were characterized by cyclic voltammetry at a scanning rate of 100 mV/s for more than 4000 cycles. All electrochemical tests were carried out on an Autolab electrochemical working station (PGSTAT 302N).

Calculation Methods. For the three-electrode system, the specific capacitance of rGO/RuO_2-X was calculated on the basis of galvanostatic charge/discharge tests according to

$$C_s = \frac{\int i\,\mathrm{d}V}{2m\Delta V(\mathrm{d}V/\mathrm{d}t)}$$

while the specific capacitance of RuO_2 only was calculated on the basis of cyclic voltammetry tests according to

$$C_{s,RuO_2} = \frac{\int i_{rGO/RuO_2}\,\mathrm{d}V - \int i_{rGO}\,\mathrm{d}V}{2m_{RuO_2}\Delta V(\mathrm{d}V/\mathrm{d}t)}$$

where ΔV is the applied voltage window, i is the current, $\mathrm{d}V/\mathrm{d}t$ is the scanning rate, m is the total weight of rGO/RuO_2-X, and and m_{RuO_2} is the weight of RuO_2 nanoparticles only.

For the two-electrode system, the specific capacitance of rGO/RuO_2-X was calculated on the basis of galvanostatic charge/discharge tests according to

$$C_s = 2\frac{it}{m\Delta V}$$

where i and t are the discharge current and time, ΔV is the drop in potential during discharge, and m is the weight of the active materials present on one single electrode. The energy density and power density were calculated from $E = (^1/_4)(^1/_2)C_s\Delta V^2$ and $P = E/t$.

Since $C_s = C_{s,rGO}(\text{wt \% rGO}) + C_{s,RuO_2}(\text{wt \% } RuO_2)$, individual contributions of rGO and RuO_2 to the energy density were calculated accordingly.

■ ASSOCIATED CONTENT

Supporting Information

The Supporting Information is available free of charge on the ACS Publications website at DOI: 10.1021/acsami.5b04704.

STEM photograph of rGO/RuO_2-50; particle size distribution of rGO/RuO_2-(15−50); XRD and Raman spectra of RuO_2, CCC-rGO, and CC-rGO/RuO_2-50; O 1s XPS spectra; RuO_2 ALD functionalization; CV measurements of CC, CC-rGO (before and after O_3 treatment), and rGO/RuO_2-50; charge/discharge measurements of CC-rGO and CC-rGO/RuO_2-20; and Ragone plots of energy density vs power density (PDF)

■ AUTHOR INFORMATION

Corresponding Authors

*E-mail fyang@nanogune.eu (F.Y.).
*E-mail mknez@nanogune.eu (M.K.).

Notes

The authors declare no competing financial interest.

■ ACKNOWLEDGMENTS

We acknowledge financial support by the Spanish Ministry of Economy and Competitivity (MINECO) through Project

DOI: 10.1021/acsami.5b04704
ACS Appl. Mater. Interfaces 2015, 7, 20513−20519

MAT2012-38161 and the Basque government through Project PI2013-56. M.K. acknowledges financial support through Marie Curie Actions (CIG) within Project 322158 (ARTEN). C.R. acknowledges financial support from the Basque Department of Education (Grant No. IT-621-13) and the Spanish Government (Grant No. MAT2013-46593-C6).

REFERENCES

(1) Weiss, N. O.; Zhou, H.; Liao, L.; Liu, Y.; Jiang, S.; Huang, Y.; Duan, X. Graphene: An Emerging Electronic Material. *Adv. Mater.* **2012**, *24*, 5782−5825.
(2) Choi, H.-J.; Jung, S.-M.; Seo, J.-M.; Chang, D. W.; Dai, L.; Baek, J.-B. Graphene for Energy Conversion and Storage in Fuel Cells and Supercapacitors. *Nano Energy* **2012**, *1*, 534−551.
(3) Tan, Y. B.; Lee, J.-M. Graphene for Supercapacitor Applications. *J. Mater. Chem. A* **2013**, *1*, 14814−14843.
(4) Zhang, L. L.; Zhou, R.; Zhao, X. S. Graphene-Based Materials as Supercapacitor Electrodes. *J. Mater. Chem.* **2010**, *20*, 5983−5992.
(5) Kim, S. J.; Choi, K.; Lee, B.; Kim, Y.; Hong, B. H. Materials for Flexible, Stretchable Electronics: Graphene and 2D Materials. *Annu. Rev. Mater. Res.* **2015**, *45*, 63−84.
(6) Xie, G.; Zhang, K.; Guo, B.; Liu, Q.; Fang, L.; Gong, J. R. Graphene-Based Materials for Hydrogen Generation from Light-Driven Water Splitting. *Adv. Mater.* **2013**, *25*, 3820−3839.
(7) Zhang, Y. I.; Zhang, L.; Zhou, C. Review of Chemical Vapor Deposition of Graphene and Related Applications. *Acc. Chem. Res.* **2013**, *46*, 2329−2339.
(8) Zhu, Y.; Murali, S.; Cai, W.; Li, X.; Suk, J. W.; Potts, J. R.; Ruoff, R. S. Graphene and Graphene Oxide: Synthesis, Properties, and Applications. *Adv. Mater.* **2010**, *22*, 3906−3924.
(9) Beidaghi, M.; Gogotsi, Y. Capacitive Energy Storage in Micro-Scale Devices: Recent Advances in Design and Fabrication of Micro-Supercapacitors. *Energy Environ. Sci.* **2014**, *7*, 867−884.
(10) Zhang, Q.; Uchaker, E.; Candelaria, S. L.; Cao, G. Nanomaterials for Energy Conversion and Storage. *Chem. Soc. Rev.* **2013**, *42*, 3127−3171.
(11) Zhi, M.; Xiang, C.; Li, J.; Li, M.; Wu, N. Nanostructured Carbon-Metal Oxide Composite Electrodes for Supercapacitors: A Review. *Nanoscale* **2013**, *5*, 72−88.
(12) Simon, P.; Gogotsi, Y. Materials for Electrochemical Capacitors. *Nat. Mater.* **2008**, *7*, 845−854.
(13) Wang, S.; Dryfe, R. A. W. Graphene Oxide-Assisted Deposition of Carbon Nanotubes on Carbon Cloth as Advanced Binder-Free Electrodes for Flexible Supercapacitors. *J. Mater. Chem. A* **2013**, *1*, 5279−5283.
(14) Wang, Y.; Shi, Z.; Huang, Y.; Ma, Y.; Wang, C.; Chen, M.; Chen, Y. Supercapacitor Devices Based on Graphene Materials. *J. Phys. Chem. C* **2009**, *113*, 13103−13107.
(15) Liu, C.; Yu, Z.; Neff, D.; Zhamu, A.; Jang, B. Z. Graphene-Based Supercapacitor with an Ultrahigh Energy Density. *Nano Lett.* **2010**, *10*, 4863−4868.
(16) Yu, G.; Hu, L.; Liu, N.; Wang, H.; Vosgueritchian, M.; Yang, Y.; Cui, Y.; Bao, Z. Enhancing the Supercapacitor Performance of graphene/MnO_2 Nanostructured Electrodes by Conductive Wrapping. *Nano Lett.* **2011**, *11*, 4438−4442.
(17) Mitra, S.; Lokesh, K. S.; Sampath, S. Exfoliated Graphite−ruthenium Oxide Composite Electrodes for Electrochemical Supercapacitors. *J. Power Sources* **2008**, *185*, 1544−1549.
(18) Wu, Z.-S.; Wang, D.-W.; Ren, W.; Zhao, J.; Zhou, G.; Li, F.; Cheng, H.-M. Anchoring Hydrous RuO_2 on Graphene Sheets for High-Performance Electrochemical Capacitors. *Adv. Funct. Mater.* **2010**, *20*, 3595−3602.
(19) Zhang, C.; Zhou, H.; Yu, X.; Shan, D.; Ye, T.; Huang, Z.; Kuang, Y. Synthesis of RuO_2 Decorated Quasi Graphene Nanosheets and Their Application in Supercapacitors. *RSC Adv.* **2014**, *4*, 11197−11205.
(20) Knez, M.; Nielsch, K.; Niinistö, L. Synthesis and Surface Engineering of Complex Nanostructures by Atomic Layer Deposition. *Adv. Mater.* **2007**, *19*, 3425−3438.
(21) George, S. M. Atomic Layer Deposition: An Overview. *Chem. Rev.* **2010**, *110*, 111−131.
(22) Kim, W.-H.; Park, S.-J.; Kim, D.; Kim, H. Atomic Layer Deposition of Ruthenium and Ruthenium-Oxide Thin Films by Using a $Ru(EtCp)_2$ Precursor and Oxygen Gas. *J. Korean Phys. Soc.* **2009**, *55*, 32−37.
(23) Yim, S.-S.; Lee, D.-J.; Kim, K.-S.; Kim, S.-H.; Yoon, T.-S.; Kim, K.-B. Nucleation Kinetics of Ru on Silicon Oxide and Silicon Nitride Surfaces Deposited by Atomic Layer Deposition. *J. Appl. Phys.* **2008**, *103*, 113509.
(24) Kwon, O.-K.; Kim, J.-H.; Park, H.-S.; Kang, S.-W. Atomic Layer Deposition of Ruthenium Thin Films for Copper Glue Layer. *J. Electrochem. Soc.* **2004**, *151*, G109−G112.
(25) Park, S.-J.; Kim, W.-H.; Lee, H.-B.-R.; Maeng, W. J.; Kim, H. Thermal and Plasma Enhanced Atomic Layer Deposition Ruthenium and Electrical Characterization as a Metal Electrode. *Microelectron. Eng.* **2008**, *85*, 39−44.
(26) Hong, T. E.; Choi, S.-H.; Yeo, S.; Park, J.-Y.; Kim, S.-H.; Cheon, T.; Kim, H.; Kim, M.-K.; Kim, H. Atomic Layer Deposition of Ru Thin Films Using a Ru(0) Metallorganic Precursor and O_2. *ECS J. Solid State Sci. Technol.* **2013**, *2*, P47−P53.
(27) Pinna, N.; Knez, M. *Atomic Layer Deposition of Nanostructured Materials*; Wiley−VCH: Weinheim, Germany, 2011.
(28) Tong, X.; Qin, Y.; Guo, X.; Moutanabbir, O.; Ao, X.; Pippel, E.; Zhang, L.; Knez, M. Enhanced Catalytic Activity for Methanol Electro-Oxidation of Uniformly Dispersed Nickel Oxide Nanoparticles-Carbon Nanotube Hybrid Materials. *Small* **2012**, *8*, 3390−3395.
(29) Puurunen, R. L.; Vandervorst, W. Island Growth as a Growth Mode in Atomic Layer Deposition: A Phenomenological Model. *J. Appl. Phys.* **2004**, *96*, 7686−7695.
(30) Kim, K.; Lee, H.-B.-R.; Johnson, R. W.; Tanskanen, J. T.; Liu, N.; Kim, M.-G.; Pang, C.; Ahn, C.; Bent, S. F.; Bao, Z. Selective Metal Deposition at Graphene Line Defects by Atomic Layer Deposition. *Nat. Commun.* **2014**, *5*, 4781.
(31) Han, J. T.; Jeong, B. H.; Seo, S. H.; Roh, K. C.; Kim, S.; Choi, S.; Woo, J. S.; Kim, H. Y.; Jang, J. I.; Shin, D.-C.; Jeong, S.; Jeong, H. J.; Jeong, Y. S.; Lee, G. W. Dispersant-Free Conducting Pastes for Flexible and Printed Nanocarbon Electrodes. *Nat. Commun.* **2013**, *4*, 2491.
(32) Hu, C.-C.; Chen, W.-C. Effects of Substrates on the Capacitive Performance of $RuO_x{\cdot}nH_2O$ and Activated carbon−RuO_x Electrodes for Supercapacitors. *Electrochim. Acta* **2004**, *49*, 3469−3477.
(33) Chen, L. Y.; Hou, Y.; Kang, J. L.; Hirata, A.; Fujita, T.; Chen, M. W. Toward the Theoretical Capacitance of RuO_2 Reinforced by Highly Conductive Nanoporous Gold. *Adv. Energy Mater.* **2013**, *3*, 851−856.
(34) Soin, N.; Roy, S. S.; Mitra, S. K.; Thundat, T.; McLaughlin, J. A. Nanocrystalline Ruthenium Oxide Dispersed Few Layered Graphene (FLG) Nanoflakes as Supercapacitor Electrodes. *J. Mater. Chem.* **2012**, *22*, 14944−14950.
(35) Lang, X.; Hirata, A.; Fujita, T.; Chen, M. Nanoporous Metal/oxide Hybrid Electrodes for Electrochemical Supercapacitors. *Nat. Nanotechnol.* **2011**, *6*, 232−236.
(36) Hu, C.-C.; Chen, W.-C.; Chang, K.-H. How to Achieve Maximum Utilization of Hydrous Ruthenium Oxide for Supercapacitors. *J. Electrochem. Soc.* **2004**, *151*, A281−A290.

DOI: 10.1021/acsami.5b04704
ACS Appl. Mater. Interfaces 2015, 7, 20513−20519